ENG. Struct. Civ. Eng. 2026, 20(4): 736–756
https://doi.org/10.1007/s11709-026-1299-3

RESEARCH ARTICLE

Cold-formed steel under fire: Dual testing and empirical strength modeling

Fatih Mehmet ÖZKAL[a*], Casim YAZICI[b], Suleyman Nazif ORHAN[c], Burak Kaan CIRPICI[c]

[a] *Department of Civil Engineering, Atatürk University, Erzurum 25240, Türkiye*
[b] *Department of Construction, Ağrı İbrahim Çeçen University, Ağrı 04400, Türkiye*
[c] *Department of Civil Engineering, Erzurum Technical University, Erzurum 25050, Türkiye*
[*] *Corresponding author. E-mail: fmozkal@atauni.edu.tr*

ABSTRACT This research investigates the structural behavior of cold-formed steel (CFS) under elevated temperature conditions, focusing on the response against both in-fire and post-fire effects. Through experimental analysis and empirical modeling, the study aims to specify the impact of temperature on the mechanical properties of CFS, specifically examining the changes in yield strength, ultimate tensile strength, and ultimate elongation. Tensile tests were conducted on CFS specimens of S235 and S355 grades exposed to temperatures ranging from 23 to 1000 °C, both during and after exposure to heating. Experimental findings revealed that yield strength and ultimate tensile strength decreased by up to 70% at 600 °C, 85% at 800 °C, and approximately 95% at 1000 °C during fire exposure, while post-fire conditions showed smaller decreases, with reductions of 15% at 800 °C and 30% at 1000 °C. In addition, empirical models, based on regression analysis and curve-fitting techniques, were developed to predict the yield strength variations of CFS, aiming to provide a supportive tool for predicting material behavior in fire scenarios. The empirical prediction models exhibit high accuracy in predicting post-fire conditions within a specific range of temperature, strength, and thickness but showed higher errors for in-fire conditions, emphasizing the complexity of material response under dynamic heating conditions. Validation of the prediction models involves an extensive analysis of previous studies, considering factors such as yield strength, specimen thickness, heating regimes, soaking times, and tensile loading rates. The results highlight the importance of considering especially initial yield strength and specimen thickness in predicting material behavior accurately. Overall, this research contributes to a deeper understanding of the sensitivity of steel material to elevated temperatures and provides substantial insights for enhancing fire safety assessments and structural design practices in the construction industry. The findings offer the baselines for developing more robust and reliable methodologies for evaluating structural performance in fire scenarios.

KEYWORDS cold-formed steel, fire resistance, elevated temperatures, empirical prediction model

1 Introduction

Structural deterioration occurs during numerous fire events each year, often resulting in severe injuries, loss of life, and substantial economic damage. The extent of damage and losses caused by fires is significantly influenced by factors such as the fire resistance and durability of the materials [1]. The impact of a standard fire varies significantly across different materials, leading to distinct alterations in their mechanical properties. Although steel is essentially non-combustible and exhibits high thermal conductivity (approximately 53–60 W/(m·K) at room temperature), the rapid heat transfer during fire exposure significantly influences its stress distribution and reduces its load-bearing capacity at elevated temperatures. Steel structural members exhibit high strength and stiffness under normal conditions, but their mechanical properties degrade rapidly at elevated temperatures due to increased ambient heat. Critical temperatures between 550–600 °C typically result in more than a 50% reduction in yield strength, depending on the steel's carbon content [2]. Cold-formed steel

Article history: Received May 26, 2025; Accepted Jan 5, 2026

(CFS), due to its greater slenderness and reduced buckling resistance compared to regular steel, experiences accelerated strength and rigidity losses under fire, often leading to premature structural failure [3].

Fire performance of light steel frame (LSF) and cold-formed steel frame systems varies significantly with the protection configuration and exposure scenario because of the high thermal conductivity and slenderness of steel. Experimental studies have shown that double-layer gypsum boards markedly enhance fire resistance, while insulation placement and fire exposure side critically affect failure modes [4]. Reported failure temperatures range from 400 to 650 °C, depending on load level and protection design [5], suggesting that the 350 °C limit prescribed in EN 1993-1-2 [2] may not be conservative for highly loaded or asymmetrically exposed members [6].

Light steel members, formed by cold-rolling steel sheets through forming machines, were initially utilized in the automotive, railway, and aviation industries before their application in the construction industry emerged later. CFS structures, which are expected to withstand substantial loads, present several advantages, such as a superior strength-to-self-weight ratio, ease of construction, and cost-effective design. With advancements in manufacturing techniques and the enhanced strength of materials, CFS has emerged as a favored option over conventional hot-rolled steel for constructing various types of structures [7]. However, the cold-forming process commonly results in an increase in yield stress and a decrease in ductility, particularly noticeable in the corner regions of the profiles. Material within these zones may display anisotropic characteristics and retain residual stress, contributing to unpredictable behavior in structural components [8].

Hot-rolled and CFS exhibit distinct behaviors when exposed to elevated temperatures. CFS has emerged as a crucial material in fire-prone environments due to its versatility, strength-to-weight ratio, inherent non-combustibility, structural resilience, and ease of construction. However, its performance under elevated temperatures requires strategic enhancements to meet safety and design standards [9]. In CFS the temperature at which residual strength degradation begins is lower than that observed in hot-rolled steels [10]. The use of fire-resistant sheathing, such as gypsum plasterboard and aluminum silicate cotton, has demonstrated significant improvements in the fire resistance of CFS structures, extending the failure time of components [11,12]. Several fire protection methods are used for LSF walls, such as gypsum boards, mineral wool insulation, and intumescent coatings [13]. Recent research shows that using insulation layers and increasing cavity depth can improve the insulation performance, though critical steel temperatures may still be reached under external fire exposure [14].

Additionally, advancements in predictive modeling and experimental validations have provided contribution to the fracture behavior of thin-walled CFS, enabling the design of elements capable of retaining structural integrity during and after fire exposure [15,16]. The introduction of innovative fire protection strategies, such as layering gypsum and aluminum silicate materials, minimizes thermal bridge effects and enhances durability, making CFS suitable for both residential and commercial buildings [11,17]. Furthermore, finite element modeling has been pivotal in optimizing the design of CFS members, ensuring stability under fire-induced stresses and extending usability even post-fire [18]. Lastly, research on post-fire mechanical properties highlights that strain-hardening effects in CFS members can enhance residual load-bearing capacity, although fire exposure significantly reduces overall strength [17,19]. These advancements make CFS a viable material for constructing safe and sustainable structures in fire-sensitive areas, with practical applications spanning low-rise buildings, modular constructions, and critical infrastructure [20].

The objective of this study is to investigate the behavior of CFS under elevated temperature conditions (23–1000 °C), particularly the degradation of mechanical characteristics, and to develop empirical models for predicting these changes. For this purpose, tensile coupons made from CFS grades of S235 and S355, were subjected to axial tensile tests.

The research objectives are outlined as follows.

1) Investigate the changes in yield strength, ultimate tensile strength, and ductility of CFS at elevated temperatures.

2) Compare the material behavior during and after exposure to high temperatures.

3) Develop empirical prediction models for assessing yield strength reduction based on temperature exposure.

4) Validate the developed models using data from previous studies to determine their prediction accuracy and limitations.

5) Identify the key parameters (such as steel grade, specimen thickness, and heating regime) influencing the mechanical characteristics of CFS under fire conditions.

2 Materials and testing

To determine the structural behavior changes of CFS, tensile coupons were subjected to axial tensile testing between 23 and 1000 °C. Tensile tests were conducted on specimens with a thickness of 3 mm, produced from CFS materials of S235 and S355 grades, in accordance with the ISO-834 [21] standard fire curve, at 100 °C intervals. The reason for applying the standard fire curve is to use the concept of equivalent temperature by basing it on the real fire curve, making it the closest fire effect model accepted in related regulations.

2.1 Test specimens

Two types of CFS material were subjected to testing, with three tensile coupons tested in each experimental group. S235 and S355 grades are identified also as ST37 and ST52 in Turkish codes and correspond to widely used structural steel qualities in local design practice. These steel grades are designed as low-alloy structural steels and widely used owing to their high strength and low cost as well as their favorable strength-to-weight ratios and ease of fabrication in structural engineering applications. From a material classification perspective, S235 and S355 are regarded as conventional structural steels that form an essential part of typical CFS applications in both historical practice and current design standards. S235 and S355 steels are widely used in storage rack systems, high-rise and long-span structures, industrial facilities and other manufacturing sectors requiring heavy load-carrying capacity (such as automotive and shipbuilding), and they constitute a large proportion of the steels preferred for CFS applications. Owing to their thin-walled configurations, high thermal conductivity and low buckling resistance, S235 and S355 steels are vulnerable to fire and elevated temperatures, so that their behavior and performance can be considered broadly representative of typical CFS structural applications. In addition, machinability, low carbon content, low density, weldability and corrosion resistance are also influential factors in the preference for these steel grades. The chemical compositions of S235 and S355 CFSs used in this study are shown in Table 1, while physical and mechanical characteristics are provided in Table 2.

Tensile coupons were cut in the longitudinal direction, in other words, in the direction parallel to the rolling direction of the CFS sheets, to ensure uniform material properties during testing. Prior to testing, the specimens underwent surface preparation using fine-grit sandpaper to remove oxidation and irregularities, ensuring accurate and consistent test results. Precautions were taken to avoid the formation of non-uniform heat-affected zones or mechanical deformations that might compromise the integrity of the specimens. A total of 126 tensile coupon tests were conducted for examination under and after elevated temperature effects, considering 11 temperature levels. The mechanical properties of the materials (yield strength, ultimate tensile strength, and ultimate elongation) were determined through tensile coupon tests. Tensile coupons were produced according to ASTM-E8 [22] guidelines and tested at a displacement rate of 0.3 mm/min according to ASTM-E21 [23] guidelines. The geometric properties of the tensile coupons are provided in Fig. 1.

2.2 Elevated temperature effects

The heating procedure for the exposure of the test

Table 1 Chemical compositions of S235 and S355 CFSs (weight in %)

Structural steel grade	C	Cu	N	Mn	P	S	Si
S235	0.17	0.55	0.012	1.40	0.040	0.040	0.25
S355	0.24	0.55	0.012	1.60	0.035	0.035	0.55

Table 2 Physical and mechanical characteristics of S235 and S355 CFSs

Physical and mechanical characteristics	S235	S355
Yield strength (MPa)	235–355	355–500
Tensile strength (MPa)	360–510	490–650
Elongation (%)	20–25	16–20
Impact toughness (J at 20 °C)	27	27
Density (g/cm^3)	7.85	7.85
Melting point (°C)	1420–1460	1420–1460
Thermal conductivity (W/mK at 20 °C)	50.2	48.3
Thermal expansion coefficient (μm/(m·°C) at 20 °C)	11.7	11.7

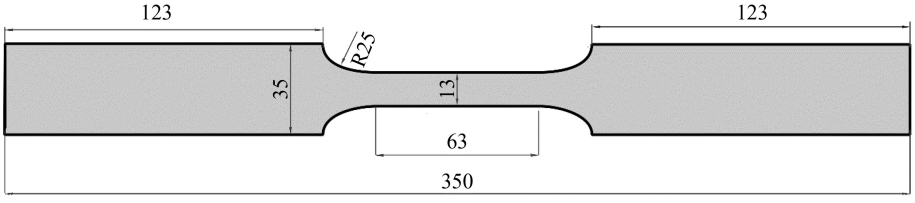

Fig. 1 Details of tensile test coupons (unit: mm).

specimens to elevated temperature effects were performed using two types of temperature-controlled electric furnaces. Both furnaces were equipped with thermocouples to monitor and control the heating temperature. This stage was conducted under two separate conditions: in-fire and post-fire behaviors by the application of the ISO-834 [21] standard fire curve, which provides a nominal representation of fully developed compartment fires. The ISO-834 standard defines the so-called standard temperature–time curve used primarily to assess the fire resistance of structural members in buildings and is generally associated with a fully developed cellulosic fire scenario, conceptually similar to the ASTM E119 [24] building fire curve [25,26]. Within the framework of EN 1993-1-2 [2], this curve corresponds to the standard temperature–time curve type of nominal fire exposure. Hydrocarbon fire curves, such as ASTM E1529 [27], reach higher peak temperatures with a much faster heating rate and are not considered in the present study. During all heating phases, the furnace temperature was continuously recorded by the built-in thermocouples so that the actual thermal exposure could be compared with the theoretical ISO-834 temperature–time relationship. Using this curve ensures that the heating rate and temperature–time relationship are representative of realistic fire exposure, while maintaining comparability with other experimental and regulatory studies [25,28,29]. In this way, the time-dependent heating rate prescribed by ISO-834 inherently captures the evolution of temperature in a fully developed cellulosic fire within the assumptions of nominal fire exposure. Because this rate is standardized and accepted in EN 1993-1-2 [2] and other design guidelines, adopting it allows the test data to be directly applicable to engineering fire design and to rational assessments of in-fire and post-fire structural behavior.

Highest target temperature was determined as 1000 °C based on previous research to achieve comparable results. The heating regimes of natural fires in buildings typically depend on standard fire conditions, considering factors such as the environment, density of combustible materials, and ventilation within or around the structures [29]. The selected temperature range from 23 to 1000 °C reflects realistic and widely accepted building-fire scenarios, as it encompasses both the onset of thermal degradation and the extreme upper limits observed in fully developed fires [30]. Selecting 1000 °C as the maximum temperature is particularly relevant for industrial scenarios where structural steel components in high-risk facilities, such as petrochemical plants, may experience extreme localized heating during severe fire events [31]. Furthermore, the ISO-834 standard fire curve approaches a plateau near 1000 °C, which supports the selection of this upper limit [32]. Such conditions demand precise modeling of material behavior to enhance the reliability of fire safety designs. Additionally, this temperature limit aligns with fire safety standards, as most engineering fire scenarios involve temperature exposures that peak below or around 1000 °C, even under the most severe conditions [29]. CFS members, owing to their thin-walled geometry and high thermal conductivity, can heat up rapidly during fires, and their post-fire mechanical degradation becomes critical especially beyond 600 °C, where yield strength reductions become pronounced. Real or natural fires may reach temperatures ranging from 500 to above 1200 °C depending on ventilation and fuel load [25], and therefore assessing material behavior up to 1000 °C provides a representative upper bound for structural fire analysis [28]. This range meets the practical needs of performance-based design by capturing all critical thermal phases from ambient conditions to irreversible material deterioration, and also ensures compliance with fire safety regulations.

Although it is claimed by Li and Young [33] and Yan et al. [10] that the heating rate has a minimal impact on the post-fire mechanical properties of CFSs, as long as the soak time is sufficiently long to ensure temperature stability and uniformity within the specimens; outcomes of this study and also the evaluation of previous studies proves an opposite conclusion. Furthermore, the ISO-834 temperature–time curve is considered a closely adequate fire model accepted within relevant regulations and is one of the most commonly used furnace exposures in fire resistance testing when natural fires are assumed. The influence of ventilation condition and thermal properties of surrounding structures may also be taken into account by adjusting/modifying the time scale to assess the fire resistance of structural members [25,32].

For the purpose of obtaining the difference between the temperatures of specimens and furnaces, special tensile coupons apart from test specimens were prepared by drilling holes at the two ends of the reduced sections of the coupons for both in-fire and post-fire tests considering the regulations of ASTM-E21 [23]. The specimen temperatures measured by K-type nickel-chromium thermocouples mounted in the holes to measure the real-time steel surface temperature by the average readings during both of the heating and cooling processes. Considering the cross-checking results between the furnaces and thermocouples, the temperature readings from the specimen-mounted thermocouples, which were independent from the furnace control system, indicated a consistent offset of 10–20 °C relative to the internal temperature of the furnaces. Heating and cooling curves within the experimental investigation are provided in Fig. 2.

Azhari et al. [34] concluded that in cooling tests conducted after elevated temperature exposure on CFS s, water-cooling at temperatures of 700 °C and above would have a greater effect on the steel structure and residual

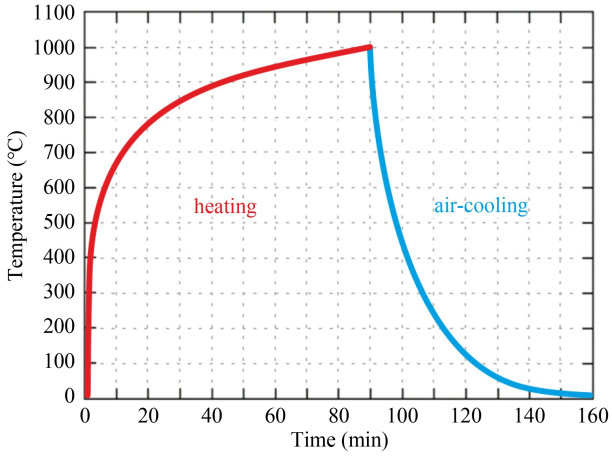

Fig. 2 Heating and air-cooling curves.

steel strength compared to air-cooling. Piloto et al. [35] evaluated the mechanical properties of structural steel specimens at room temperature after being subjected to fire-like conditions followed by different cooling rates, such as natural air cooling and quenching. Their findings indicated that the yield strength of the specimens could become either lower or higher than the original room-temperature value, depending on both the maximum fire temperature and the cooling rate. Lu et al. [36] mentioned that in the behavior of Q235, Q345, and Q420 steel samples heated up to 700 °C after a fire, the effect of water-cooling or air-cooling could be neglected. Sajid and Kiran [37] stated that after elevated temperature tests on ASTM A36 steels, significant changes in the microstructure of the steel occurred starting from temperatures after 600 °C under the same cooling conditions. Li et al. [38] and Kang et al. [31] mentioned in their studies on Q690 steels to determine the properties remaining after temperature exposure that while air cooling starting from 700 °C had a very low effect, cooling tests starting from temperatures after 700 °C significantly affected the steel structure. Özkal et al. [39] emphasized the dramatic change in the mechanical properties of structural steel after 600 °C in a study where they investigated the effects of high temperatures by applying air-cooling. Yan et al. [10] conducted air-cooling to determine the post-fire strengths of high-strength CFSs and identified 700 °C as the limit temperature where the effect of cooling would be significant.

Natural air cooling was performed instead of alternative methods due to its closer resemblance to real-world fire scenarios. While rapid cooling through water immersion can quickly reduce temperatures, formation of steep thermal gradients leads to significant microstructural changes, residual stresses, and distortions in steel, as reported in previous studies [31,40]. In contrast, air cooling facilitates a more gradual temperature reduction, minimizing these adverse effects. This approach ensures that the residual mechanical properties observed in the experiments more accurately reflect conditions experienced by structural components after fire exposure.

The mechanical properties of steels are commonly assessed through tensile coupon tests, which can be performed using either the steady-state or transient state test method. While the transient state test method is deemed more realistic due to its ability to simulate real fire behavior, including the creep effect, the steady-state test method is preferred for its simplicity and direct provision of continuous stress-strain curves [26,41]. In this approach, specimens are heated to the predetermined temperature levels and subjected to a constant-rate tensile load until failure, while maintaining a constant temperature [42]. This method is also advantageous for potential analyses of complex structural fire resistance in the future [43]. The steady-state test method was chosen for this research due to its practicality. Regarding in-fire behavior, tensile load was applied on the test specimens as soon as the target temperatures are achieved. In the same manner for post-fire behavior, once the target temperature was reached, the test specimens were immediately removed from the furnace and left to cool naturally in the air.

In fact, ASTM-E21 [23] suggests that the duration of holding at temperature before the test should be determined by the time required for the specimen to reach equilibrium. Unless specified otherwise, this duration should not be less than 20 min. However, the impact of heating duration can be disregarded, given that the heating time is sufficiently long to ensure uniform temperature distribution within the steel sample [36,44,45]. Gao et al. [46] also stated that the cooling method and the duration of exposure to elevated temperatures has minimal impact on the mechanical properties of the material according to the analysis of previous studies. According to another perspective provided by Smith et al. [45], heating a steel section above 600 °C for an extended period, exceeding 1 h, may lead to some strength loss due to spheroidization of the pearlite. This refers to a microstructural alteration in which the lamellar iron carbides within the pearlite amalgamate into particles that then grow larger over time. At temperatures surpassing 723 °C, the pearlite initiates a transformation back to austenite, and the ferrite grains begin to coarsen, typically in an irregular fashion. When the steel is heated to temperatures well above 723 °C and subsequently air-cooled, there is minimal overall alteration in the observed microstructure, with the exception of changes in grain size.

Hence, the influence of these factors was disregarded in this study and there was no waiting period after reaching the target temperature to ensure a stable correlation between the tensile behavior of the specimens which were tested under and after elevated temperature effects. Moreover, any soaking-time was not preferred in order to

prevent additional stress formation during heating within the in-fire test specimens. During the heat treatment process for post-fire tests, tensile coupons were supported on ceramic roller supports to provide thermal isolation by preventing interaction between them, ensuring that thermal expansion was maintained. Figure 3 depicts the heating processes of test specimens inside the electric furnaces for in-fire and post-fire tests.

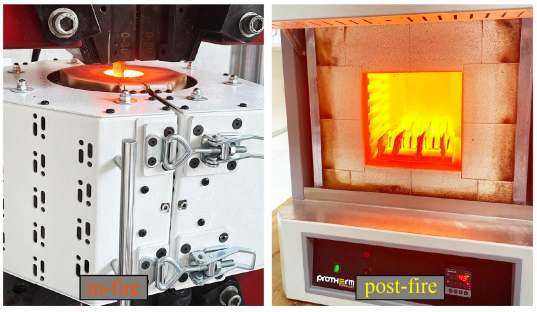

Fig. 3 Application of elevated temperature effects on tensile coupons: heating process for in-fire and post-fire testing.

2.3 Tensile testing procedure

Axial tensile tests were conducted on the specimens under strain control at a constant displacement rate of 0.3 mm/min, both under and after exposure to elevated temperature effects. The strain rate remained unchanged in both the elastic and plastic regions. 0.3 mm/min displacement rate corresponds to a strain rate of approximately 0.005 (mm/mm)/min, which is within the range of 0.005 ± 0.002 (mm/mm)/min as specified by ASTM-E21 [23]. Load measurements were recorded using a digital load-cell integrated into the tensile test machine, featuring a capacity of 200 kN and an accuracy of ±0.5%. Strain data were directly transformed from displacement values by the built-in measurement system of the machine, which provides a sensitivity of ±0.01 mm.

Alongside a conventional electric furnace for tensile tests after heating exposure, another electric furnace with an internal volume of 60 mm × 200 mm, capable of accommodating the tensile testing apparatus, was used to conduct tests during elevated temperature effects. Regarding the in-fire tests, thermal expansion of the test coupons was allowed by maintaining zero tensile load during the heat exposure. Once the target temperature was reached, tensile load was then applied to the specimens. Prior to the post-fire tensile tests, following the specimens cooling down to room temperature, any oxidation present on the surface of the coupons was eliminated using sandpaper. The applied tension load and the strain on tensile coupon specimens were continuously recorded through the high-precision internal load-cell and physical extensometer of the same tensile test machine used in the post-fire tests. Data acquisition was performed in real time using the built-in digital controller of the load–displacement system. The relationship between the behaviors of specimens tested under and after elevated temperature effects, obtained through these tests, conducted within the scope of the study, will enable the prediction of the behavior characteristics of large-volume structural members. Tensile tests conducted on the specimens both during and after exposure to elevated temperature effects are presented in Fig. 4.

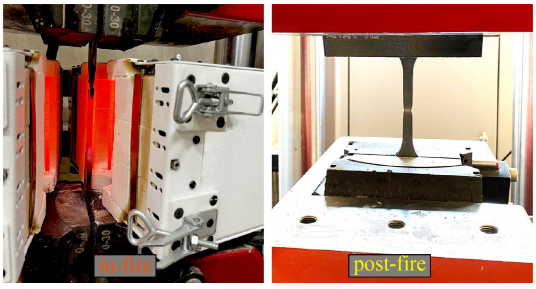

Fig. 4 Tensile coupon tests during and after exposure to elevated temperature effects.

3 Results and discussion

To ensure the reliability of the experimental results, statistical analysis was initially conducted. For each temperature condition, three specimens were tested; mean values and coefficients of variation (COV) were computed. The experimental results and reduction factors of residual yield strength, ultimate tensile strength, and ultimate elongation for the tensile coupons are presented in Tables 3–5, while the changes in their structural characteristics are comparatively illustrated for S235 and S355 CFSs in the subsections. Regarding the comparison of the test results achieved in this study with previous research, they are compatible with the general evaluation of Sidey and Teague [47] that the reduction in mechanical properties at elevated temperatures for CFSs is typically 10%–20% greater than that observed for hot-rolled steels, owing to the differences in metallurgical composition and molecular surface effects.

In the tables and graphs, F_y, F_u, and ε_u represents yield strength, ultimate tensile strength and ultimate elongation, respectively. These values are provided separately for S235 and S355 CFS, both during (in-fire) and after (post-fire) exposure to elevated temperature effects, by averaging the numerical outcomes of three specimens at the same temperature. In Tables 3 and 4, the COV ranges provided for each temperature level offer a compact statistical measure of the scatter in F_y, F_u, and ε_u for both steel grades. In general, these COV ranges increase progressively with temperature, indicating that the variability of the mechanical response becomes more pronounced as the specimens undergo more severe

Table 3 Tensile test results for S235 and S355 CFS during heating (in-fire)

Temperature (°C)	S235			S355			COV range (%)
	F_y (MPa)	F_u (MPa)	ε_u (%)	F_y (MPa)	F_u (MPa)	ε_u (%)	
23	359.8	442.5	22.26	433.9	552.1	18.79	0.7–1.3
100	347.4	444.3	22.06	421.7	557.2	19.33	1.0–1.7
200	321.5	465.7	21.52	387.9	573.4	18.19	1.2–2.4
300	298.3	492.4	20.28	346.8	598.3	17.20	1.3–3.0
400	254.1	443.8	18.12	283.3	536.2	15.49	1.4–3.8
500	208.1	326.4	15.27	197.1	376.1	13.38	1.7–4.5
600	149.8	194.2	12.53	142.8	212.1	10.21	1.8–5.6
700	83.5	107.8	10.37	90.1	119.7	7.78	2.1–6.9
800	48.8	58.8	8.71	54.3	68.5	6.33	2.4–8.1
900	31.8	37.5	7.95	36.0	45.6	5.71	2.7–8.9
1000	16.9	20.3	7.14	21.8	24.1	5.00	3.0–9.6

Table 4 Tensile test results for S235 and S355 CFS after heating (post-fire)

Temperature (°C)	S235			S355			COV range (%)
	F_y (MPa)	F_u (MPa)	ε_u (%)	F_y (MPa)	F_u (MPa)	ε_u (%)	
23	359.8	442.5	22.26	433.9	552.1	18.79	0.7–1.3
100	357.7	451.9	22.33	439.1	552.4	18.86	1.1–1.7
200	360.7	446.8	22.68	434.1	562.5	19.13	1.2–2.3
300	357.1	443.9	22.58	432.6	555.0	18.80	1.2–2.6
400	351.1	445.4	22.68	440.3	551.5	19.11	1.2–2.5
500	359.3	448.1	23.27	437.6	552.4	19.62	0.9–2.7
600	356.6	442.5	23.91	431.9	543.2	20.34	1.5–2.5
700	349.6	427.8	24.57	411.9	514.9	21.02	1.7–2.8
800	339.5	409.7	25.15	380.8	468.0	22.06	1.9–3.6
900	322.1	381.2	26.43	342.8	416.7	23.07	1.9–4.1
1000	304.6	346.4	28.18	303.8	371.8	25.26	2.2–4.8

Table 5 Reduction factors for mechanical properties of S235 and S355 CFS

Temperature (°C)	In-fire						Post-fire					
	S235			S355			S235			S355		
	$k_{0.2}$	k_u	k_ε	$k_{0.2}$	k_u	k_ε	$k_{0.2}$	k_u	k_ε	$k_{0.2}$	k_u	k_ε
23	1.000	1.000	1.000	1.000	1.000	1.000	1.000	1.000	1.000	1.000	1.000	1.000
100	0.966	1.004	0.991	0.972	1.009	1.029	0.994	1.021	1.003	1.012	1.001	1.004
200	0.894	1.052	0.967	0.894	1.039	0.968	1.003	1.010	1.019	1.000	1.019	1.018
300	0.829	1.113	0.911	0.799	1.084	0.915	0.992	1.003	1.014	0.997	1.005	1.001
400	0.706	1.003	0.814	0.653	0.971	0.824	0.976	1.007	1.019	1.015	0.999	1.017
500	0.578	0.738	0.686	0.454	0.681	0.712	0.999	1.013	1.045	1.009	1.001	1.044
600	0.416	0.439	0.563	0.329	0.384	0.543	0.991	1.000	1.074	0.995	0.984	1.082
700	0.232	0.244	0.466	0.208	0.217	0.414	0.972	0.967	1.104	0.949	0.933	1.119
800	0.136	0.133	0.391	0.125	0.124	0.337	0.944	0.926	1.130	0.878	0.848	1.174
900	0.088	0.085	0.357	0.083	0.083	0.304	0.895	0.861	1.187	0.790	0.755	1.228
1000	0.047	0.046	0.321	0.050	0.044	0.266	0.847	0.783	1.266	0.700	0.673	1.344

thermal degradation. Among the key parameters, F_u systematically exhibits the lowest COV values, whereas ε_u shows the highest scatter, reflecting the greater sensitivity of ductility to local imperfections and microstructural heterogeneity. In addition, S355 tends to display slightly higher COV ranges than S235, which is consistent with the higher temperature sensitivity of high-strength CFSs discussed below. When comparing in-fire and post-fire conditions, the COV ranges remain relatively small after exposure, whereas during fire exposure they increase more markedly at high temperatures, highlighting the combined influence of simultaneous heating and loading on the stability of the tensile response.

In terms of the reduction factors in Table 5, yield strength at 0.2% strain is $k_{0.2} = f_{y,T}/f_y$, ultimate tensile strength is $k_u = f_{u,T}/f_u$, and ultimate elongation is $k_\varepsilon = \varepsilon_{u,T}/\varepsilon_u$. The yield strength, ultimate tensile strength, and ultimate elongation values exhibit similar changes for S235 and S355 grade steels during exposure to elevated temperature effects, while the changes observed in these values after exposure are more pronounced for S355 grade. Overall, the results indicate that both steel grades exhibit different levels of sensitivity to elevated temperatures, with the heating process leading to a decrease in material characteristics but in-fire conditions causing even further decreases. It has also been observed that steel grades with superior material characteristics are affected more severely by in-fire condition than post-fire condition, and are prone to exhibit more dramatic deterioration.

High-strength steels tend to exhibit greater temperature sensitivity than lower-strength grades, primarily due to their metastable microstructural features and the

strengthening mechanisms activated during manufacturing [43]. In cold-formed applications, the enhanced strength of S355 is largely achieved through high dislocation densities and elevated levels of residual stress introduced by cold working, and in some cases through alloying or heat-treatment routes [48]. When exposed to elevated temperatures, this metastable structure becomes less stable. Recovery, recrystallization and tempering of cold-worked regions then progressively relax dislocations and residual stresses at relatively lower temperatures, compared with the degradation thresholds observed in lower-strength ferrite–pearlite steels [49]. As high temperatures remove the additional strength gained from cold-forming and heat treatment [30,50], high-strength steels experience proportionally larger permanent strength losses, which manifests as a higher sensitivity to temperature compared with conventional S235 grade steels.

From a fire design perspective, the experimental results indicate that the load-bearing capacity of S235 and S355 CFS members becomes critical once steel temperatures approach approximately 550–600 °C. Although existing design provisions for structural carbon steel, such as EN 1993-1-2 [2], often associate temperatures around 350 °C with conservative limits for the onset of strength degradation, the combined in-fire and post-fire test results of this study show that, for thin CFS members, a pronounced and rapid loss of yield and ultimate tensile strength occurs above about 600 °C, with in-fire reductions reaching up to roughly 70% at 600 °C and more severe degradation at higher temperatures. At the same time, the residual (post-fire) mechanical properties remain close to the ambient-temperature values up to roughly 600 °C and then begin to deteriorate more rapidly. Therefore, for unprotected CFS members subjected to standard fire exposure, temperatures beyond approximately 600°C should be treated as a critical threshold for in-fire structural resistance, while fire scenarios that expose the steel to temperatures above about 800 °C (when no load-bearing function during the fire is assumed) should be regarded as causing severe and potentially irreversible degradation of the residual mechanical properties.

3.1 Tensile behavior

The stress-strain curve trends of the tensile coupons tested after heat exposure show no significant alterations except for test values, in contrast to those tested during heat exposure. Therefore, the stress-strain curves for only the specimens tested during elevated temperature exposure are presented in Figs. 5 and 6. For each elevated-temperature level, three tensile coupons were tested; however, only one stress-strain curve is presented in these figures. The displayed curve corresponds to the specimen whose behavior most closely represents the average response of the three tests at that temperature.

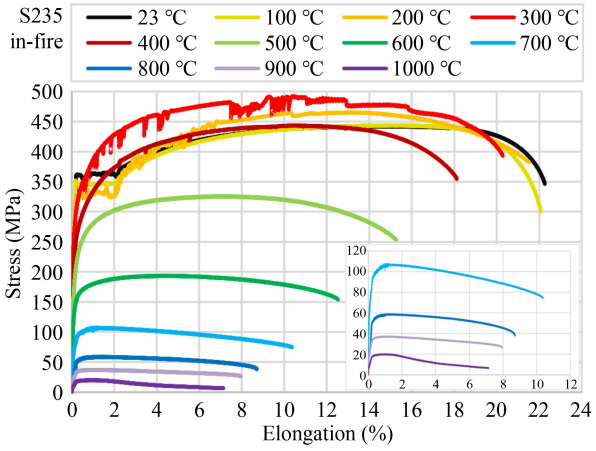

Fig. 5 Stress–strain curves of the S235 tensile coupons tested during heating.

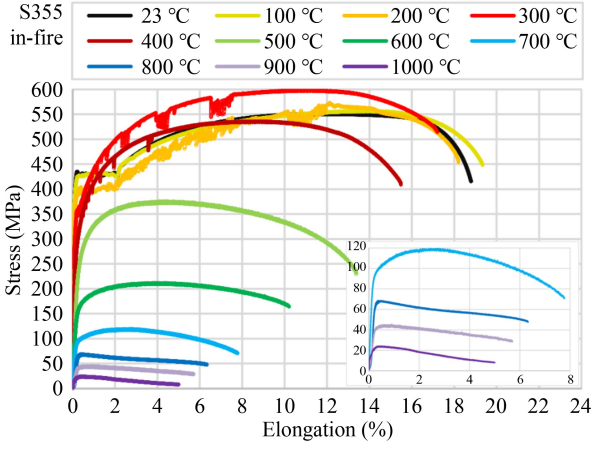

Fig. 6 Stress-strain curves of the S355 tensile coupons tested during heating.

For both S235 and S355 grade tensile coupons tested after heat exposure (post-fire), the stress-strain curves of specimens exposed to temperatures ranging from 23 to 600 °C exhibit a similar pattern, featuring a linear elastic region followed by a distinct yield plateau. Beyond 700 °C, size of the yield plateau gradually increases as the slope of the linear region diminishes, up to 1000 °C. Concurrently, height of the plastic region is lowered, indicating a decrease in the ratio of ultimate strength to yield strength. In addition, a general trend observed is that both yield strength and ultimate strength decrease with increasing temperature, while ultimate elongation tends to increase. This pattern highlights the reduced capacity of the CFS after heating exposure to withstand heavier loads but increased ductility at higher temperatures.

Considering tensile strength tests conducted during exposure to elevated temperatures (in-fire), notable alterations in stress–strain curves become apparent.

Initially, only the curves of specimens tested at ambient and 100 °C exhibit a linear elastic region followed by a distinct yield plateau, with these two curves appearing nearly identical. However, at 200 °C, the size of the yield plateau significantly diminishes alongside a reduction in ultimate strength, and sudden drops in tensile stress that resemble saw-teeth in the plastic region. By 300 °C, the yield plateau almost entirely disappears, though the saw-teeth resemblance remains discernible, disappearing only at 500 °C. Following 600 °C, the downward slope of the curve's tail beyond the ultimate strength point gradually increases, and the linear region until the yield strength begins to draw an S shape after 800 °C. Ultimately, the rupture moment becomes nearly indiscernible from the curve at 1000 °C.

These changes in the stress–strain curves indicate a gradual transition from ductile to brittle behavior as the temperature increases. At low temperatures, the presence of a distinct yield plateau, a relatively long plastic region and a gradual post-peak softening are characteristic of a ductile response. With increasing temperature, as described above, the yield plateau shrinks and disappears, the plastic region becomes shorter, the post-peak branch steepens and the in-fire ultimate elongation drops markedly, especially above 600–800 °C. In summary, the loss of a stable yield plateau, the reduction in in-fire ultimate elongation and the suppression of necking in the high-temperature curves clearly demonstrate that CFS gradually shifts from ductile to brittle behavior under severe thermal exposure.

For the in-fire tests, the pronounced reduction in tensile strength observed at temperatures above 800 °C (up to about 95%) can be attributed to high-temperature phase transformations and microstructural degradation in carbon steel. In this range, the original ferrite-pearlite microstructure progressively transforms to austenite, carbides dissolve and the pearlitic lamellae break down [45], while significant grain coarsening and recovery processes remove most of the dislocation barriers that sustain the room-temperature strength [51]. For thin CFS coupons, these metallurgical changes are further intensified by severe surface oxidation and local section loss, especially as the temperature approaches 1000 °C. The oxidation-induced damage and flaking of the outer layer reduce the load-carrying cross-section of the steel, so that the combined effects of phase transformation, softening and oxidation provide a consistent explanation for the very low hot strengths measured at the highest temperature levels.

Based on the previously provided test results, there is a general tendency for the yield strength and ultimate strength to decrease with increasing temperature, except for the increase in ultimate strength observed between 200 and 400 °C, whereas ultimate elongation decreases under in-fire conditions but increases under post-fire conditions. Between 200 and 400 °C, the increased scatter observed in Figs. 5 and 6 is associated with the transition region in which CFSs partially lose their yield plateau while not yet developing a fully temperature-softened response. At around 300 °C, the material exhibits mixed and unstable characteristics: the yield plateau becomes unstable or disappears, and the initial nonlinearity becomes more pronounced. Previous studies have shown that the yield plateau observed between 20 and 200 °C in CFS vanishes at approximately 300 °C, reflecting unstable mechanical behavior in this temperature range [48]. In addition, the marked variability near 300 °C is influenced by the well-known phenomenon of blue brittleness occurring between 200 and 450 °C, during which the formation of a blue oxide film is accompanied by discontinuous yielding [49]. The saw-tooth stress drops commonly seen in this range arise from repeated pinning and unpinning of moving dislocations by carbon and nitrogen atoms, producing highly unstable deformation behavior [52]. Even though the yield plateau almost disappears at 300 °C, this discontinuous yielding pattern is still observed [44], indicating an active and unstable interaction between plasticity and strain-hardening mechanisms.

3.2 Yield strength

Yield strength results for S235 and S355 CFS at different temperatures during and after the heating process, provided in Fig. 7, represent the mean values obtained from three tensile coupons tested under identical conditions. For specimens that exhibit a yield plateau, the yield strength was defined as the lower boundary of the yield plateau, which is a more stable and less test-sensitive definition of the yield strength [53,54]. This approach is consistent with practices in post-fire mechanical testing, as the upper yield stress can be highly sensitive to testing-machine stiffness and alignment according to ASTM-E8 [22]. EN 1993-1-1 [55] allows the upper yield stress to be used; however, cold-formed and high-temperature-exposed steels often deviate from the classical yield-plateau behavior.

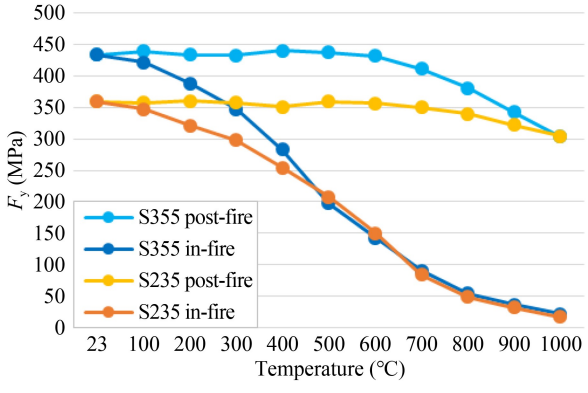

Fig. 7 Yield strength results for S235 and S355 CFS.

For specimens that do not display a yield plateau, the yield strength was determined using a residual strain level of 0.2% offset same as the technique of previous researchers [33,38,41,50,54,56]. The 0.2% proof stress is determined by the intersection of the stress−strain curve with a line drawn parallel to the initial elastic modulus. This line originates at a strain value of 0.2% and extends until it intersects the curve, representing the stress at which permanent deformation begins, as outlined in ASTM-E8 [22] guidelines.

In addition, the stress at 2.0% strain ($f_{2.0}$) is often used to describe the material response in the plastic range, complementing the conventional 0.2% proof stress ($f_{0.2}$). At elevated temperatures, steels typically lose a clear yield plateau, and stresses corresponding to fixed strain levels (e.g., $f_{0.2}$, $f_{0.5}$, $f_{1.5}$, $f_{2.0}$) are therefore adopted as practical strength indicators [41]. However, especially for CFSs, yield stresses at higher strain levels (1.5%–2.0%) may approach the ultimate strength, making them unsafe for design purposes if used as yield criteria [30]. According to ASTM-E8 [22] and EN 1993-1-2 [2], the 0.2% proof stress should be used as the design yield strength for cold-formed thin-walled members under fire, since local buckling can occur while the material is still in the elastic range before reaching 2.0% strain.

Both S235 and S355 CFSs exhibit similar trends in yield strength reduction with increasing temperature during the heating process. However, S355 generally shows more degradation compared to S235 until 600 °C with respect to their behaviors at room temperature, indicating a relatively higher weakness of the material's microstructure as temperature rises. Yield strength exhibits a continuous decrease from 100 °C onwards during exposure to elevated temperature effects, while a decrease begins at 600 °C after exposure. Regarding in-fire condition, yield strength reduction at 600 °C is 58.4% for S235 and 67.1% for S355, while that is nearly 95% at 1000 °C for both of the grades.

After exposure to elevated temperatures, both S235 and S355 CFSs experience significant reductions in yield strength, while the reduction begins after 600 °C. As the most dramatic deterioration, yield strength reduction at 1000 °C is 15.4% for S235 and 30.0% for S355 considering the post-fire condition.

3.3 Ultimate strength

The comparison between the behavior of S235 and S355 CFSs during and after the heating process reveals interesting insights. Ultimate strength results for S235 and S355 CFS at different temperatures during and after the heating process, provided in Fig. 8, represent the mean values obtained from three tensile coupons tested under identical conditions.

Both steel grades experience similar trends in ultimate strength across all temperature ranges considering in-fire condition. After an increase observed up to 300 °C during exposure to elevated temperature effects, a decreasing trend is noted, followed by a decrease starting from 600 °C after exposure. It is seen that ultimate strength is higher than the initial ultimate strength until 400 °C, by exhibiting increase of 11.3% for S235 and 8.4% for S355 at 300 °C. Afterwards, S355 CFS exhibits barely lower values compared to initial ultimate strength with respect to S235 as the temperature rises. Finally, ultimate strength reduction at 1000 °C is more than 95% during heating for both of the grades.

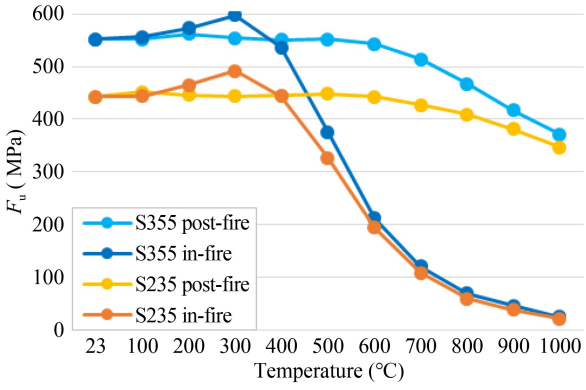

Fig. 8 Ultimate strength results for S235 and S355 CFS.

Regarding post-fire condition, ultimate strength variations of both S235 and S355 CFSs resemble yield strength variations. Despite there is no significant change on the mechanical properties of test specimens until 600 °C as expected, ultimate strength reduction at 1000 °C is 21.7% for S235 and 32.7% for S355. While both grades experience a reduction in post-fire tests after 600 °C, S355 CFS demonstrates proportionally higher decrease compared to S235 CFS, revealing a similar behavior with in-fire tests.

To have a different look on the tensile strength characteristics of the test specimens, ratio of ultimate strength to yield strength across all temperatures is illustrated in Fig. 9. This ratio represents another way to define the height of the plastic region from the yield strength level and remains consistent for the test specimens evaluated after exposure to various temperature levels. However, the ratio begins to increase for specimens tested while heating once temperatures exceed 200 °C, which actually marks the beginning of the disappearance of the yield plateau.

3.4 Ultimate elongation

Ultimate elongation reduction trends of in-fire and post-fire conditions demonstrates opposite behaviors. Ultimate elongation results prior to the rupture of the tensile test coupons for S235 and S355 CFS at different temperatures during and after the heating process, provided in Fig. 10,

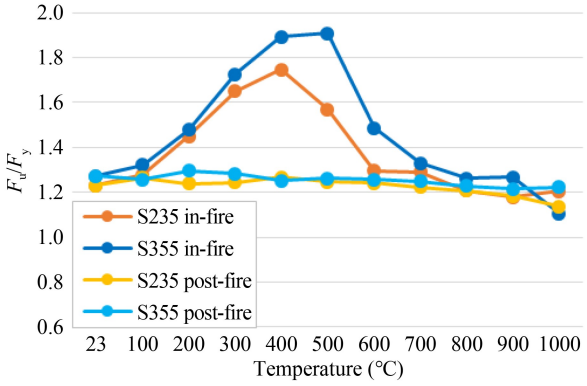

Fig. 9 Ratio of ultimate strength to yield strength across all temperatures.

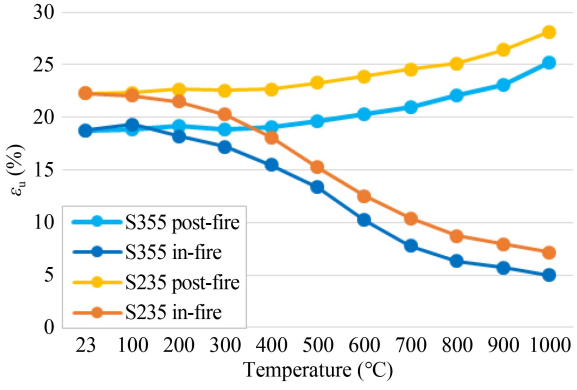

Fig. 10 Ultimate elongation results for S235 and S355 CFS.

represent the mean values obtained from three tensile coupons tested under identical conditions. These values refer exclusively to the mechanical tensile elongation measured during the tension test rather than any thermal expansion occurring during heating.

Ultimate elongation exhibits contrasting behavior during and after exposure to elevated temperature effects. Regarding in-fire tests, both S235 and S355 CFSs experience a gradual decrease in ultimate elongation as the temperature rises. However, S355 CFS generally exhibits more reduction compared to S235 CFS after 600 °C, indicating a slightly higher susceptibility to deformation under elevated temperatures. While average elongation reduction of S235 and S355 is almost 45% at 600 °C, it is 67.9% for S235 and 73.4% for S355 at 1000 °C, which indicates obvious materialization of embrittlement.

Considering post-fire tests, both S235 and S355 CFSs demonstrate an increase after 400 °C in ultimate elongation compared to their respective values at room temperature. Notably, S355 CFS consistently exhibits higher increment compared to S235 CFS at all post-fire temperatures, indicating its ability to gain more ductility after exposure to elevated temperatures. Ultimate elongation increase at 1000°C is 26.6% for S235 and 34.4% for S355.

These opposite trends in ultimate elongation between in-fire and post-fire conditions reflect both the nature of the test methods and the thermal response of CFS [51]. In in-fire tests, the material is simultaneously subjected to high temperature and mechanical loading, so thermal softening and progressive damage occur while the available ductility is rapidly consumed under sustained stress, leading to a marked reduction in ultimate elongation [26]. In addition, rate-sensitive effects associated with blue brittleness and discontinuous yielding further limit the plastic deformation capacity in this regime [52]. In contrast, in post-fire tests, the coupons are heated and then cooled without mechanical loading, so that the influence of the maximum temperature is manifested mainly through microstructural changes such as recovery, tempering of cold-worked regions, grain coarsening and the thermal relaxation of cold-forming-induced residual stresses and high dislocation densities [45,57]. These processes permanently increase ductility and explain the observed gain in residual ultimate elongation. The higher-strength S355 grade, which accumulates greater levels of residual stress and dislocation density during manufacturing [43], therefore exhibits a more pronounced increase in post-fire ultimate elongation than S235, whereas under in-fire loading both grades experience a significant loss of ductility due to the combined effects of thermal softening, rate-sensitive instability phenomena and damage accumulation [49].

3.5 Visual observation after heat exposure

The visual observations revealed differences among the test specimens exposed to various elevated temperatures. As the temperatures increased, particularly between 100 and 300 °C, the surfaces of the specimens became darker but relatively clean with respected to higher temperatures. As the exposure temperature increased, the post-fire color of the specimens began to appear blue, particularly starting from 400 °C, by becoming more evident up to 600 °C. At 700 °C, alongside the quite dark color, stains and rusts were observed on the surfaces of specimens, which consisted of iron oxides. Ash began to form on the surfaces of specimens due to the outer layer diffraction, especially for the specimens that reached temperatures equal to or above 800 °C, resulting in serious damage to the surface oxide film. The surface appearance of the in-fire test specimens is mostly similar to that of the post-fire specimens. Figure 11 illustrates the surface conditions of tensile coupons after exposure to elevated temperature effects.

The surface color and the appearance of the oxide layer on steel could serve as valuable indicators for estimating the temperatures experienced by steel members and evaluating damage after fire accidents. In the heat treatment process of steel, blue embrittlement may occur

Fig. 11 Surface conditions of the tensile coupons prior to post-fire tests.

at a specific temperature due to the prevention of dislocations by carbon and nitrogen atoms, resulting in an increase in the material's strength [58]. Low-temperature embrittlement occurs due to an increase in the critical stress required for dislocation movement [59]. Similar to findings from previous studies, steel exhibits a blue coloration at a temperature of 400 °C due to oxidation, indicating the onset of blue brittleness [52]. Blue brittleness describes the phenomenon where steel takes on a blue hue and the oxidation also affects the corrosion rate. Observations show that the surfaces of specimens become rougher when exposed to elevated temperatures due to oxidation. Additionally, the color darkens at temperatures exceeding 600 °C. It is noteworthy to mention that diffraction/flaking and extensive softening has been observed on the outer layers of the tensile coupons, gradually beginning at temperature of 700 °C. This phenomenon is attributed to the oxidation of the outer layer [52] due to the microstructural changes focusing on the tempered martensite layer on the surface, which is influenced by the chemical composition of the materials [39]. Outer layer diffraction was mentioned in many previous studies by stating that the initial formation temperature is 600−800 °C for steel. For the purpose of emphasizing blue brittleness phenomenon at 400−600 °C range and almost charred microstructure of the specimens at 1000 °C, tensile coupons with thicker cross-sections after in-fire testing are depicted in Fig. 12.

3.6 Visual observation after tensile strength tests

The failure modes of tensile coupons in both steel grades (S235 and S355) resemble each other but flaking on the surfaces of S355 CFS tensile coupons are less obvious with respect to S235 CFS. Besides, failure modes of the specimens are significantly influenced by in-fire and post-fire conditions, as well as naturally by elevated temperature levels.

The necking phenomenon observed after tensile tests serves as a significant indicator of the impact of test parameters. While this phenomenon is consistent for both steel grades, it occurs distinctly depending on the heating conditions. Figure 13 provides the failure mode representations of the tensile coupons after in-fire tests, revealing that the shrinkage of the fracture section becomes less noticeable with increasing temperature, particularly beyond 600 °C. Toughness and deformability of the specimens string along with this change. However, necking at failure remains highly stable in specimens tested after exposure to elevated temperatures and necking is still evident even at 1000 °C for post-fire test specimens. Decreasing ultimate elongation results of in-fire tests and increasing results of post-fire tests that may be defined as a kind of tempering effect support this outcome regarding the ductility of the specimens.

According to the observations of Smith et al. [45], when heating structural steels, there is a slight increase in strength observed for temperatures up to 250 °C. However, as the temperature rises beyond this point, the yield or proof stress gradually declines. Distortion will

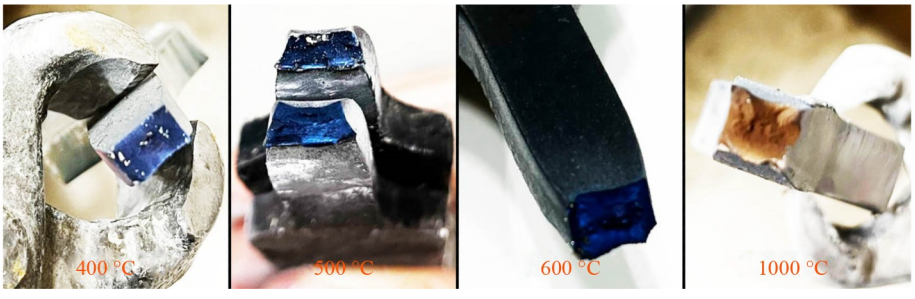

Fig. 12 Cross-sections of the tensile coupons after in-fire tests.

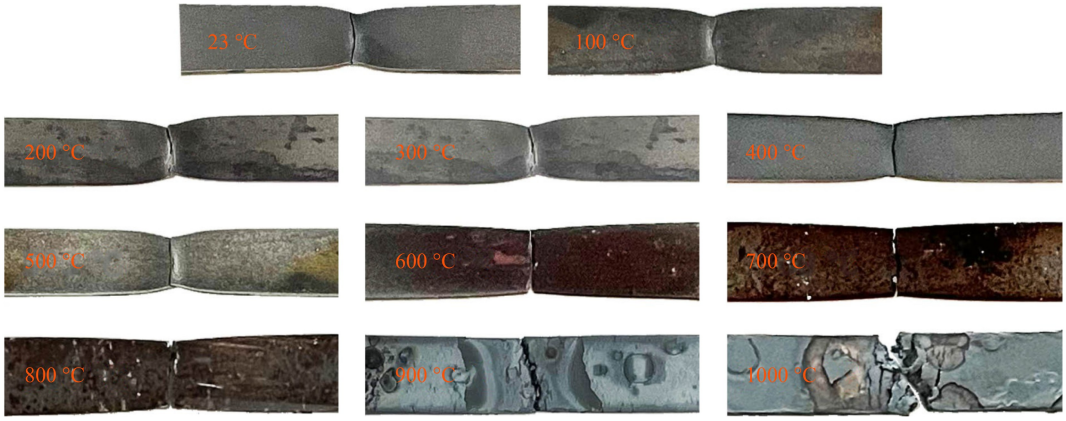

Fig. 13 Failure mode representations of the tensile coupons after in-fire tests.

start to occur when the flow stress drops below the design stress or the actual load applied. In addition, Dolzhenkov [52] remarks that a blue oxide film forms on the metal surface during mechanical tests or deformation of steel at elevated temperatures. Beside this, strength increases while plasticity and ductility decrease. Blue brittleness is most pronounced after rolling or during mechanical tests at temperatures associated with blue brittleness, indicating the combined influence of plastic deformation and temperature. When plastic deformation and elevated temperature occur at different times, the effect of blue brittleness is significantly reduced. Elevated temperature effects after exposure increases the ductility against the embrittlement during exposure on test specimens in this study. Especially the deterioration of plasticity capacity due to the simultaneous effect of elevated temperatures and deformation is compatible with the findings of previous studies.

4 Empirical prediction models

Based on the data obtained from tensile tests, empirical prediction models have been developed to predict the changes in material characteristics depending on the elevated temperature levels. The models have been formulated on the averaged forms of nonlinear interpolation considering yield strength variation of the tested CFS specimens in terms of the elevated temperature exposure. These empirical prediction models, developed separately for the behavior during and after exposure to elevated temperatures, have the potential to enable the incorporation of fire effects into numerical models created for future structural analyses involving CFS.

The application of a cubic polynomial model was preferred considering its ability to effectively capture the nonlinear relationship between temperature level and mechanical characteristics of steel, especially at critical temperature thresholds. Previous studies indicate that the degradation in tensile strength of steel typically exhibits a nonlinear trend, driven by microstructural transformations and phase changes resulting from elevated temperature exposure [33,37,54,60]. The cubic polynomial offers the necessary flexibility to represent these complex behaviors by allowing changes in slope and curvature across different temperature ranges, while minimizing the risk of overfitting, making it a widely accepted method in structural engineering applications [33,54].

4.1 Formulation of the Prediction Models

Empirical models have been developed as a function of temperature to predict the changes in yield strengths of S235 and S355 grade CFS depending on the elevated temperature levels. However, based on both the data obtained in the current study and the results from previous studies, it is apparent that the material behavior becomes significantly unstable after 800 °C. Therefore, the definition range of the models has been set from 23 to 800 °C. In real-world fire events, temperatures in structural components typically reach up to about 800 °C before complete material failure [36]. Beyond this level, CFS undergoes severe degradation with strength losses often exceeding 90%, rendering its mechanical properties unreliable for structural purposes. For this reason, both the formulation and validation of the proposed models focus on the practical range of 23–800 °C, which covers the temperature spectrum relevant for engineering fire design.

The first empirical model developed for the residual yield strength after exposure to elevated temperatures and air-cooling is as follows:

$$f_{\mathrm{y,post-fire}}^{\mathrm{T}} = f_{\mathrm{y}}^{23}(-6\times10^{-10}\times T^{3}+3\times10^{-7}\times T^{2} +2\times10^{-5}\times T+0.99),\ \ 23\ ^{\circ}\mathrm{C}\leqslant T\leqslant 800\ ^{\circ}\mathrm{C}, \tag{1}$$

Similarly, the second empirical model developed for the yield strength during exposure to elevated temperatures is as follows:

$$f_{\mathrm{y,in-fire}}^{\mathrm{T}} = f_{\mathrm{y}}^{23}(2.75\times10^{-9}\times T^{3}-4\times10^{-6}\times T^{2} +3.7\times10^{-4}\times T+0.99),\ \ 23\ ^{\circ}\mathrm{C}\leqslant T\leqslant 800\ ^{\circ}\mathrm{C}. \tag{2}$$

In the developed models, yield strength of the material at ambient temperature, denoted as f_y^{23}, and the elevated temperature level (T) are defined. Normalizing the cubic polynomials by f_y^{23} ensures that the models reproduce the reference yield strength at ambient temperature and then describe a fully nonlinear degradation curve over the 23–800 °C range. The cubic polynomial model allows the regression functions to represent the global nonlinear trend of strength degradation across all temperature intervals considered.

The comparison of the actual yield strength values obtained from axial tensile tests for both models and the calculated error percentages alongside the absolute average errors are presented in Tables 6 and 7 regarding the numerical outcomes of this study.

The higher prediction errors observed above 500 °C in the in-fire tests are partly related to the unstable mechanical response of CFSs in the transitional temperature range; however, they also arise from the inherent limitations of the third-order approximation used in the predictive model. At higher temperature levels, processes such as grain coarsening, recrystallization, and phase transformations introduce variability in the mechanical responses of the material, which increases the scatter and steepens the degradation curve of the strength-temperature relationship. This rapid curvature change reduces the prediction ability of a cubic polynomial, leading to increased fitting errors. Moreover, significant redistribution of residual stresses occurs in this range, further influencing the mechanical characteristics and reducing the accuracy of empirical models [37,54]. Similar trends have been reported in studies investigating residual mechanical properties of steel exposed to fire, where transitional temperature zones consistently exhibit higher prediction errors [33,60]. Future improvements on the prediction approaches could include incorporating additional parameters and detailed microstructural evolution, also using higher-order or piecewise formulations to enhance model accuracy.

Table 6 Empirical model estimations after exposure to elevated temperatures (post-fire)

Temperature (°C)	S235			S355		
	f_y^{exp} (MPa)	f_y^{emp} (MPa)	Error (%)	f_y^{exp} (MPa)	f_y^{emp} (MPa)	Error (%)
23	359.8	356.4	+0.94	433.9	429.8	+0.94
100	357.7	357.8	–0.03	439.1	431.5	+1.74
200	360.7	360.2	+0.12	434.1	434.4	–0.06
300	357.1	362.2	–1.45	432.6	436.9	–0.98
400	351.1	362.5	–3.26	440.3	437.2	+0.70
500	359.3	359.8	–0.13	437.6	433.9	+0.85
600	356.6	352.7	+1.08	431.9	425.4	+1.50
700	349.6	340.1	+2.73	411.9	410.1	+0.43
800	339.5	320.5	+5.59	380.8	386.5	–1.49
Average	–	–	1.70	–	–	0.97

Table 7 Empirical model estimations during exposure to elevated temperatures (in-fire)

Temperature (°C)	S235			S355		
	f_y^{exp} (MPa)	f_y^{emp} (MPa)	Error (%)	f_y^{exp} (MPa)	f_y^{emp} (MPa)	Error (%)
23	359.8	358.5	+0.36	433.9	432.4	+0.36
100	347.4	356.1	–2.51	421.7	429.5	–1.83
200	321.5	333.2	–3.62	387.9	401.8	–3.59
300	298.3	293.3	+1.67	346.8	353.7	–1.99
400	254.1	242.5	+4.57	283.3	292.5	–3.23
500	208.1	186.6	+10.29	197.1	225.1	–14.18
600	149.8	131.7	+12.12	142.8	158.8	–11.23
700	83.5	83.6	–0.12	90.1	100.8	–11.85
800	48.8	48.2	+1.10	54.3	58.1	–7.06
Average	–	–	4.04	–	–	6.15

Regarding the evaluation on the experimental results of this study, the following outcomes can be inferred based on the empirical models developed for predicting the yield strength of CFS materials at various temperature levels and the associated prediction percentages.

1) In the empirical model developed for post-elevated temperature effects, the average prediction error considering both S235 and S355 CFS was calculated to be 1.34%, indicating highly successful predictions with a maximum error of 5.59%.

2) While prediction errors exceeding 10% are noticeable in the empirical model developed for the materials under elevated temperature effects, particularly in the range of 500–700 °C, the average prediction error considering both S235 and S355 CFS is calculated to be 5.09%, indicating an acceptable prediction success.

4.2 Validation of the prediction models

To validate the proposed empirical prediction models for widespread use and determine the limitation ranges, a total of 20-three previous studies were analyzed, encompassing both post-fire and in-fire situations. Factors such as the type and yield strength of the steel material, the thickness of the test specimens, the heating regime, the soaking period after reaching the target temperature, and the loading rate for the tensile strength tests were considered in the validation process. Yield strength results of the test specimens were taken into account across the temperature range of 23–800 °C regarding the reference studies.

While this study primarily used experimental data from the literature for the validation, external data from construction projects were not incorporated. This is

because data from previous studies provide results under controlled experimental setups with well-documented parameters such as heating rates, soaking periods, and loading conditions. These allow for consistent validation of the empirical models. External data from construction projects are often influenced by additional variables, such as environmental factors and unquantified thermal gradients, which are outside the scope of the empirical models developed in this study.

The average prediction error for each study was calculated, along with the tendency for overestimation or underestimation. The concept information and prediction errors for the studies on post-fire testing are provided in Tables 8 and 9. Prediction errors are also presented in

Table 8 Predictions for the previous studies (after exposure to elevated temperatures)

Study	Type	Yield strength (MPa)	Thickness (mm)	Heating rate (°C/min)	Soaking time (min)	Loading rate (/min)	Error (%)	Prediction tendency
Recent study	S235	360	3.00	ISO-834	0	0.005	1.70	negative
	S355	434	3.00	ISO-834	0	0.005	0.97	negative
Chiew et al. [43]	S690	769	8.00	30	10	0.003	13.21	positive
Gunalan and Mahendran [61]	G300	352	1.00	10–20	50–60	0.0125	15.80	positive
	G500	664	1.15	10–20	50–60	0.0125	79.07	positive
	G550	664	0.95	10–20	50–60	0.0125	73.26	positive
Wang et al. [56]	Q460	513	8.00	15	20	0.06	8.05	negative
Lu et al. [36]	Q235	342	7.50	15	30	0.06	2.02	negative
	Q345	389	7.50	15	30	0.06	2.38	negative
	Q420	447	7.00	15	30	0.06	1.99	negative
Li et al. [38]	Q690	803	10.00	5–20	10	0.015	18.69	positive
Gao et al. [46]	S30408	277	10.00	20	30–180	0.03	4.23	positive
	S31608	258	10.00	20	30–180	0.03	1.70	positive
Li and Young [33]	Q690	691	4.00	10	20	0.0015	13.11	negative
	Q690	673	6.00	10	20	0.0015	9.81	positive
	Q960	991	4.00	10	20	0.0015	40.25	negative
Cai and Young [28]	G550	775	0.42	40–60	15	0.007	61.64	positive
	G500	623	1.20	40–60	15	0.007	20.24	positive
	G450	513	1.90	40–60	15	0.007	25.05	positive
Tao et al. [62]	G1.4003	332	3.00	20	30	0.06	6.75	positive
	G1.4307	265	3.00	20	30	0.06	3.78	negative
	G1.4362	577	4.00	20	30	0.06	16.45	negative
	G1.4404	268	4.00	20	30	0.06	18.59	negative
	G1.4462	600	4.00	20	30	0.06	17.91	negative
Zhou et al. [63]	Q690	798	10.00	20	30	0.015	16.05	positive
Ren et al. [49]	Q235	270	1.00	25	10	0.015	9.44	negative
	Q235	306	2.00	25	10	0.015	3.87	negative
Zhang et al. [53]	Q355	446	3.00	15	120	0.02	4.60	positive
Zhang et al. [64]	Q460	676	4.00	15	120	0.017	26.59	positive
	Q690	758	4.00	15	120	0.017	12.67	positive
Zhou et al. [54]	Q620	669	5.00	15	20	0.0017	8.56	negative
Yan et al. [10]	DP-340	422	1.40	25	15–20	0.015	10.20	negative
	DP-700	744	1.40	25	15–20	0.015	29.42	positive
	MS-1030	1327	1.00	25	15–20	0.015	58.40	positive
	MS-1200	1387	1.00	25	15–20	0.015	50.27	positive
Yazici et al. [65]	S235	336	3.00	15	30	0.04	2.25	positive

Table 9 Predictions for the previous studies (during exposure to elevated temperatures)

Study	Type	Yield strength (MPa)	Thickness (mm)	Heating rate (°C/min)	Soaking time (min)	Loading rate (/min)	Error (%)	Prediction tendency
Recent study	S235	360	3.00	ISO-834	0	0.005	4.04	negative
	S355	434	3.00	ISO-834	0	0.005	6.15	positive
Chen and Young [41]	G550	601	1.00	100	9	0.006	80.80	positive
	G450	535	1.90	100	9	0.006	22.69	negative
Ranawaka and Mahendran [26]	G250	315	0.60	25	20	0.003	59.33	positive
	G250	297	0.80	25	20	0.003	22.01	positive
	G250	320	0.95	25	20	0.003	31.55	positive
	G550	675	0.60	25	20	0.003	90.54	positive
	G550	610	0.80	25	20	0.003	55.31	positive
	G550	615	0.95	25	20	0.003	57.36	positive
Kankanamge and Mahendran [42]	G250	292	1.55	20	10	0.003	22.53	positive
	G250	270	1.95	20	10	0.003	27.71	positive
	G450	536	1.50	20	10	0.003	58.08	positive
	G450	515	1.90	20	10	0.003	51.78	positive
Chiew et al. [43]	S690	817	8.00	20	10	0.003	56.84	positive
Qiang et al. [29]	S960QL	1050	5.00	50	10	0.005	20.62	negative
Li and Young [33]	Q690	743	4.00	50	20	0.009	17.55	negative
	Q690	712	6.00	50	20	0.009	16.25	negative
	Q960	1024	4.00	50	20	0.009	38.34	positive
Liang et al. [48]	Q345	406	1.50	50	20	0.06	7.05	negative
	Q345	421	2.50	50	20	0.06	8.30	positive

Figs. 14–17 with respect to the yield strength and thickness values of the test specimens. In these figures, red dots represent underestimation (negative), while green dots are for the overestimation (positive).

The most significant and comparable test parameters from the previous studies are the yield strength and thickness of the test specimens. Although the heating regime, soaking time after reaching the target temperature, and loading rate during tensile strength tests also affect the experimental outcomes, evaluating the success of the prediction models based solely on these parameters does not yield a valid interpretation. Initially, a noticeable overestimation by the prediction model is evident for test specimens with initial yield strengths exceeding 600 MPa in studies conducted after exposure to elevated temperatures. In studies conducted during exposure to elevated temperatures, underestimation becomes prominent, accompanied by a high rate of overestimation starting at 500 MPa. When evaluating based on specimen thickness for both after exposure and during exposure studies,

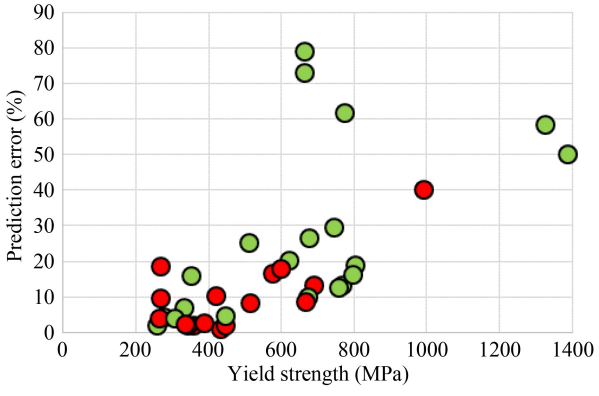

Fig. 14 Prediction errors based on yield strength after exposure to elevated temperatures.

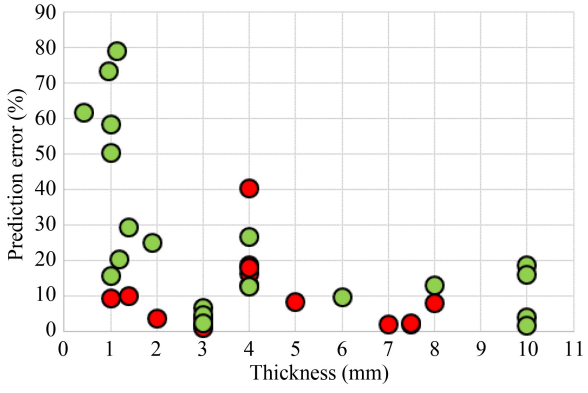

Fig. 15 Prediction errors based on thickness after exposure to elevated temperatures.

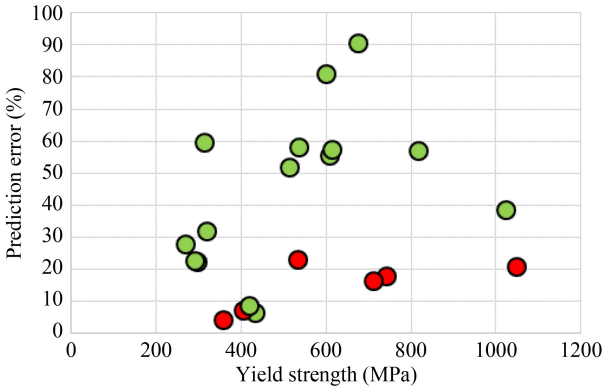

Fig. 16 Prediction errors based on yield strength during exposure to elevated temperatures.

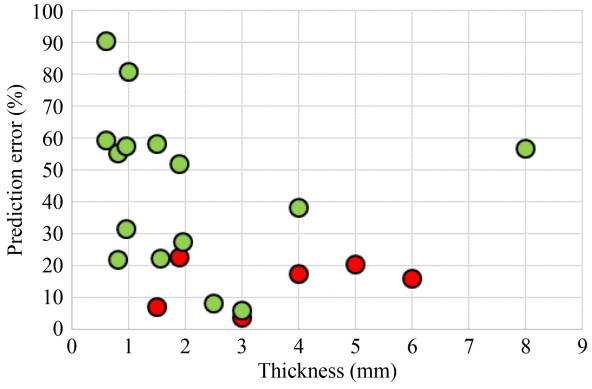

Fig. 17 Prediction errors based on thickness during exposure to elevated temperatures.

significant prediction errors due to overestimation are observed, particularly in specimens with thicknesses less than 2.0 mm. Conversely, prediction errors for thicker specimens are generally considered to be within normal ranges. This behavior can be associated with the greater sensitivity of thin, high-strength sections to thermal gradients, micro-structural variations, and local instability under fire conditions.

Consistently with these observations, the empirical prediction models exhibit higher accuracy for post-fire conditions than for in-fire conditions, because post-fire tests represent a comparatively simpler and more stable end state. In post-fire testing, the residual mechanical properties primarily reflect the effect of the maximum temperature and the associated permanent microstructural changes, including recovery, tempering and grain coarsening, which tend to relax cold-forming-induced residual stresses and produce relatively smooth and monotonic degradation trends [45]. By contrast, in-fire behavior involves simultaneous exposure to high temperature and mechanical loading, and is strongly path dependent: the response is influenced by thermal expansion and restraint, thermal softening, creep and the continuous evolution of deformation under progressively decreasing strength, as well as rate-sensitive phenomena such as blue brittleness and discontinuous yielding [26,41]. This multivariable, dynamic thermo-mechanical interaction increases the scatter and complexity of the in-fire test data, which explains why empirical formulations calibrated on global parameters provide less accurate predictions for in-fire conditions than for the more stable post-fire response.

Instead of evaluating yield strength and thickness parameters separately, their concurrent assessment offers a clearer insight into prediction success. Thickness has a more apparent effect on prediction success than yield strength; however, it is the reduction in thickness, particularly below 2.00 mm, that significantly impacts the outcomes. The combination of low thickness and high yield strength results in very high prediction errors in both after exposure and during exposure studies. Consideration of this relationship could lead to the refinement of future prediction models and contribute to more accurate assessments of structural performance under fire conditions. To illustrate this point, prediction errors are displayed in Figs. 18 and 19, which consider the ratio of yield strength to thickness, further supporting this finding.

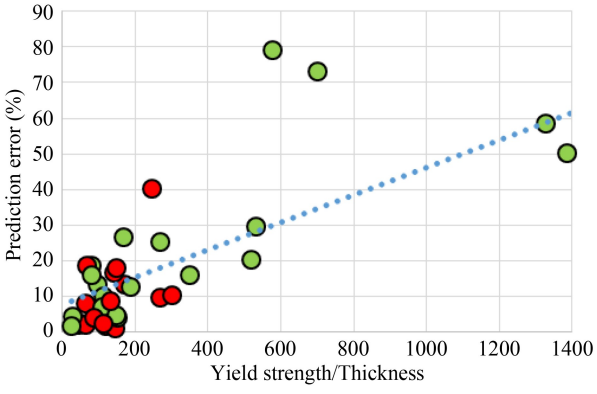

Fig. 18 Prediction errors based on yield strength/thickness ratio after exposure to elevated temperatures.

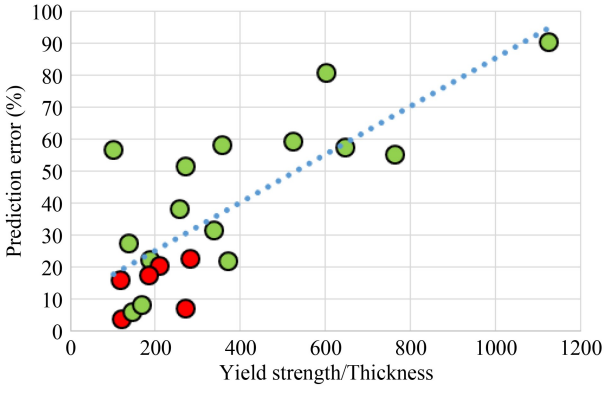

Fig. 19 Prediction errors based on yield strength/thickness ratio during exposure to elevated temperatures.

4.3 Limitations of the prediction models

Predictions regarding the residual yield strength outcomes from both the recent study and previous studies demark the limitation ranges of the empirical models. Due to the complexity of material behavior during elevated temperature effects, the second empirical model (in-fire) generally exhibits higher prediction errors compared to the first model (post-fire). Examination of various studies illustrates a notable relationship between prediction errors and both the initial yield strength and thickness values of the test specimens. Across these studies, it is evident that the magnitude of prediction errors tends to vary based on these parameters.

To propose practical prediction models, the average prediction error should be ensured to be less than 10%. Therefore, both models should be constrained such that the temperature range is between 23 and 800 °C, the yield strength at ambient temperature is lower than 800 MPa, and the thickness is higher than 2.00 mm. For thinner and higher-strength CFS members, the prediction errors observed in the validation study indicate that the proposed equations should be used with caution and interpreted as approximate envelopes rather than precise design values, and more refined member-specific analyses or additional safety margins may be required for fire resistance assessments. Correspondingly, the average prediction error is 8.58 for the first model, considering the post-fire situation, and 10.46 for the second model, considering the in-fire situation.

In cases where more accurate estimation is required for either of these models, extensive research should be performed to decrease prediction errors by refining the limitation ranges. Incorporating additional test parameters such as heating regime, soaking time, and loading rate into the empirical models could also enhance their capability for wide-ranging predictions. By integrating these factors into the empirical models, diverse conditions encountered in real-world scenarios could be accounted, thereby improving the applicability of the prediction models across a broader spectrum of situations. This expanded scope will allow for more comprehensive and reliable predictions, contributing to the advancement of fire safety engineering and materials science. Moreover, considering these additional parameters can lead to a better understanding of the complex interactions between material properties and environmental conditions, facilitating more informed decision-making in design, construction, and risk assessment processes.

Although a direct numerical comparison with the strength reduction curves given in design standards has not been carried out in this study, the proposed empirical relationships are conceptually consistent with existing design approaches for the high-temperature strength of structural carbon steel. Current code provisions and guidelines largely derive their reduction factors for in-fire conditions. Although the proposed empirical relationships were not explicitly calibrated to match these code-based strength reduction factors, the in-fire models reproduce a nonlinear degradation trend and reduction magnitudes that are broadly consistent with the general shape of such curves at moderate temperatures, while the post-fire models provide residual strengths that are, as expected, higher than the instantaneous values implied by code provisions, since they represent cooled material rather than hot strength.

5 Conclusions

Scope and content of this research offer experimental insights into the behavior of CFS under elevated temperature conditions, crucial for enhancing fire safety engineering practices and structural design methodologies. The investigation underscores the significance of understanding the material degradation of steel materials during and after fire hazards, considering the intensive impact of elevated temperatures on their structural characteristics. Through a comprehensive experimental research that focuses on the in-fire and post-fire effects, several key conclusions can be drawn.

1) The mechanical properties of CFS, such as yield strength and ultimate tensile strength, exhibit significant variations under elevated temperatures. Both S235 and S355 grades of CFS experience notable reductions in yield and ultimate strengths as temperatures rise, with more pronounced effects observed in S355 grade. Considering in-fire condition, for S235 steel, the yield strength decreased by approximately 60% at 600 °C and nearly 85% at 800 °C compared to its ambient temperature value. Similarly, for S355 steel, the yield strength dropped by approximately 65% at 600 °C and 90% at 800 °C. The post-fire condition revealed an observable degradation in tensile strength, with a reduction of approximately 10% after exposure to 800 °C.

2) Ultimate elongation demonstrated different trends: it decreased gradually during exposure to elevated temperatures, particularly above 400 °C by up to 20%. However, elongation increased after exposure, with the increase being more prominent in S355 grade by up to 35% at 800 °C.

3) It was observed that different steel grades have differential sensitivity to elevated temperatures. While both grades exhibit similar trends in material property degradation, S355 grade demonstrates a higher susceptibility to in-fire conditions, resulting in more dramatic reductions in mechanical properties compared to post-fire conditions.

4) Tensile tests conducted during exposure to elevated temperatures reveal significant alterations in stress-strain

curves, with noticeable reductions in yield and ultimate strengths, as well as changes in ductility. The necking phenomenon becomes less prominent with increasing temperature during heating, indicating reduced deformability. Blue embrittlement, flaking, and extensive softening phenomena has also been observed on the outer layers of the test specimens, gradually as the temperature rises.

5) For practical fire design, the experimental outcomes suggest that temperatures around 550–600 °C should be considered critical for the in-fire resistance of thin CFS members, whereas exposure beyond about 800 °C is associated with severe and often irreversible degradation of their residual mechanical properties.

6) Empirical prediction models have been developed to predict changes in yield strength of CFS under elevated temperature conditions. These models demonstrate high prediction accuracy for post-fire conditions, alongside acceptable prediction errors for in-fire conditions. The proposed relationships can be used to obtain temperature-dependent yield strengths for cold-formed members within the validated ranges, and then incorporated into sectional checks or numerical simulations. In this way, engineers can assess both the in-fire load-bearing capacity and the residual post-fire strength of CFS members more realistically, supporting performance-based fire design as well as rational decisions on repair, strengthening or replacement after a fire event.

7) Validation of the prediction models through analysis of previous studies on different grades of steel reveals varying degrees of prediction accuracy, influenced by factors such as yield strength and specimen thickness. The combination of low thickness and high yield strength leads to significant prediction errors, emphasizing the importance of considering these parameters in future modeling studies and indicating that current formulations should not be applied to very thin, high-strength sections without additional safety checks or refined analyses.

In summary, the findings of this study have the potential to support the future research on the behavior of CFS under elevated temperature conditions, facilitating more accurate evaluations on structural performance and fire safety in construction applications. Especially the dramatic loss in strength at temperatures beyond 800 °C proves the critical need for fire-resistant design measures in structures using CFS.

In addition, the results highlight the necessity of incorporating material-specific degradation models into fire safety standards to ensure accurate assessments of structural performance. The empirical prediction models developed in this study offer a promising tool for engineers to predict the behavior of CFS under both in-fire and post-fire scenarios, enabling more accurate structural analyses to reduce the risks associated with fire incidents.

Acknowledgements The authors would like to thank Eren Storage Racking Systems from Tekirdağ, Türkiye for providing tensile coupon specimens. This study was supported by the Scientific and Technological Research Council of Türkiye, TUBITAK (No. 122M322).

Competing interests The authors declare that they have no competing interests.

References

1. Aliş B, Yazici C, Özkal F M. Investigation of fire effects on reinforced concrete members via finite element analysis. ACS Omega, 2022, 7(30): 26881–26893
2. EN-1993. Eurocode 3–Design of steel structures—Part 1–2: General rules—Structural fire. Brussels: European Committee for Standardization, 2005
3. Cirpici B K, Orhan S N, Yazici C, Özkal F M. Numerical investigation of the fire behavior of storage rack systems protected by intumescent coating. ACS Omega, 2022, 7(40): 36001–36008
4. Piloto P A G, Khetata M S, Ramos-Gavilán A B. Analysis of the critical temperature on load bearing LSF walls under fire. Engineering Structures, 2022, 270: 114858
5. Piloto P A G, Pereira A S, Mottin A C. Fire resistance of ultra-high-strength steel columns using different heating rates. Applied Sciences, 2024, 14(11): 4887
6. Hassoune M, Kada A, Menadi B, Lamri B, Yessad O, Piloto P A G, Jiang L. Performance of single and built-up I-shaped cold formed steel stud under double sided walls fire exposure. Engineering Structures, 2025, 335: 120392
7. Çarbaş S, Taymuş R, Özdemir M. Examining the effects of different seismic base isolators on the seismic behavior of a real-size steel truss structure. Challenge Journal of Structural Mechanics, 2025, 11(2): 106–115
8. Tunca O, Erdal F, Sağsöz A E, Çarbaş S. Structural features of cold-formed steel profiles. Challenge Journal of Structural Mechanics, 2018, 4(2): 77–81
9. Sam V S, Anand N, Kumar R, Andrushia D. Influence of section profiles on flexural behavior of unsymmetrical cold-formed steel sections—Analytical and numerical investigation. Journal of Structural Fire Engineering, 2024, 5: 1–36
10. Yan X, Xia Y, Blum H B, Gernay T. Post-fire mechanical properties of advanced high-strength cold-formed steel alloys. Thin-walled Structures, 2021, 159: 107293
11. Yin L, Li R, Wang X, Chen W, Ye J, Wu X. Fire experiments on cold-formed steel square tubular columns with new gypsum sheathing configuration. Thin-walled Structures, 2024, 198: 111727
12. Dai Y, Roy K, Fang Z, Raftery G M, Ghosh K, Lim J B P. A critical review of cold-formed built-up members: Developments, challenges, and future directions. Journal of Building Engineering, 2023, 76: 107255
13. Piloto P A G, Gomes S, Torres L, Couto C, Vila Real P. Accuracy of 2D numerical models towards the prediction of the fire resistance on LSF partition walls. International Journal of Thermal Sciences, 2023, 193: 108511

14. Torres L, Couto C, Vila Real P, Piloto P. Numerical study of the fire behaviour of external walls in light steel framing. Fire Safety Journal, 2023, 141: 103946
15. Rahnavard R, Craveiro H D, Simões R A, Gardner L. Fracture behaviour of thin-walled cold-formed steel at elevated temperatures. Construction & Building Materials, 2024, 429: 136446
16. Shi Y, Wang J, Zhou X, Xue X, Li Y. Post-fire mechanical properties of Q960 cold-formed thick-walled ultra-high-strength steel. Fire Technology, 2024, 60(3): 1917–1953
17. Luo K, Li H, Yang J, Kang H, Yan F, Han X. Research on post-fire mechanical properties of thin-walled cold-formed steel and its influence on Σ-shaped columns after fire exposure. Thin-walled Structures, 2024, 204: 112315
18. Pandey M, Young B. RHS-to-RHS cold-formed S960 steel fire exposed X-joints: Structural behaviour and design. Thin-walled Structures, 2023, 188: 110711
19. Roxas C L C, Bautista C R, Dela Cruz O G, Dela Cruz R L C, De Pedro J P Q, Dungca J R, Lejano B A, Ongpeng J M C. Systematic literature review of cold-formed steel at elevated temperature scenario. Heliyon, 2023, 9(8): e19142
20. De'nan F, Yeou C Y, Salim W S W, Rahman N A, Hashim N S. Assessing cold-formed steel section performance in fire: A comprehensive review of numerical models and resistance factors. International Journal of Steel Structures, 2024, 24: 1–19
21. ISO 834-11. Fire resistance tests—Elements of building construction—Part 11: Specific requirements for the assessment of fire protection to structural steel elements. Geneva: International Organization for Standardization, 2014
22. ASTM E8/E8M-21. Standard test methods for tension testing of metallic materials. West Conshohocken, PA: ASTM, 2021
23. ASTM E21-20. Standard test methods for elevated temperature tension tests of metallic materials. West Conshohocken, PA: ASTM, 2020
24. ASTM E119-24. Standard test methods for fire tests of building construction and materials. West Conshohocken, PA: ASTM, 2024
25. Beyler C, Beitel J, Iwankiw N, Lattimer B. Fire resistance testing for performance-based fire design of buildings. Final report. 2007
26. Ranawaka T, Mahendran M. Experimental study of the mechanical properties of light gauge cold-formed steels at elevated temperatures. Fire Safety Journal, 2009, 44(2): 219–229
27. ASTM E1529-22. Standard test methods for determining effects of large hydrocarbon pool fires on structural members and assemblies. West Conshohocken, PA: ASTM, 2022
28. Cai Y, Young B. Mechanical properties of thin sheet steel after exposure to high temperatures. Thin-walled Structures, 2019, 142: 460–475
29. Qiang X, Jiang X, Bijlaard F S K, Kolstein H. Mechanical properties and design recommendations of very high strength steel S960 in fire. Engineering Structures, 2016, 112: 60–70
30. Li H T, Young B. Material properties of cold-formed high strength steel at elevated temperatures. Thin-walled Structures, 2017, 115: 289–299
31. Kang L, Suzuki M, Ge H, Wu B. Experiment of ductile fracture performances of HSSS Q690 after a fire. Journal of Constructional Steel Research, 2018, 146: 109–121
32. Wickstrom U. Application of the standard fire curve for expressing natural fires for design purposes. Technical report SP-RAPP1986:19. 1986.
33. Li H T, Young B. Residual mechanical properties of high strength steels after exposure to fire. Journal of Constructional Steel Research, 2018, 148: 562–571
34. Azhari F, Heidarpour A, Zhao X L, Hutchinson C R. Mechanical properties of ultra-high strength (Grade 1200) steel tubes under cooling phase of a fire: An experimental investigation. Construction & Building Materials, 2015, 93: 841–850
35. Piloto P A G, Vila Real P, Mesquita L, Vaz M A P. Steel mechanical properties evaluated at room temperature after being submitted at fire conditions. In: Housing construction—An interdisciplinary task. Coimbra: XXX IAHS World Congress on Housing proceedings, 2002.
36. Lu J, Liu H, Chen Z, Liao X. Experimental investigation into the post-fire mechanical properties of hot-rolled and cold-formed steels. Journal of Constructional Steel Research, 2016, 121: 291–310
37. Sajid H U, Kiran R. Influence of stress concentration and cooling methods on post-fire mechanical behavior of ASTM A36 steels. Construction & Building Materials, 2018, 186: 920–945
38. Li G Q, Lyu H, Zhang C. Post-fire mechanical properties of high strength Q690 structural steel. Journal of Constructional Steel Research, 2017, 132: 108–116
39. Özkal F M, Polat M, Yağan M, Öztürk M O. Mechanical properties and bond strength degradation of GFRP and steel rebars at elevated temperatures. Construction & Building Materials, 2018, 184: 45–57
40. Outinen J, Mäkeläinen P. Mechanical properties of structural steel at elevated temperatures and after cooling down. Fire and Materials, 2004, 28(2-4): 237–251
41. Chen J, Young B. Experimental investigation of cold-formed steel material at elevated temperatures. Thin-walled Structures, 2007, 45(1): 96–110
42. Kankanamge N D, Mahendran M. Mechanical properties of cold-formed steels at elevated temperatures. Thin-walled Structures, 2011, 49(1): 26–44
43. Chiew S P, Zhao M S, Lee C K. Mechanical properties of heat-treated high strength steel under fire/post-fire conditions. Journal of Constructional Steel Research, 2014, 98: 12–19
44. Tao Z, Wang X Q, Uy B. Stress–strain curves of structural and reinforcing steels after exposure to elevated temperatures. Journal of Materials in Civil Engineering, 2013, 25(9): 1306–1316
45. Smith C I, Kirby B R, Lapwood D G, Cole K J, Cunningham A P, Preston R R. The reinstatement of fire damaged steel framed structures. Fire Safety Journal, 1981, 4(1): 21–62
46. Gao X, Zhang X, Liu H, Chen Z, Li H. Residual mechanical properties of stainless steels S30408 and S31608 after fire exposure. Construction & Building Materials, 2018, 165: 82–92
47. Sidey M P, Teague D P. Elevated Temperature Data for Structural Grades of Galvanised Steel. British Steel (Welsh Laboratories) report. 1988
48. Liang Z, Wang W, Wang Z. Effect of cold-form and tensile strain rate on mechanical properties of Q345 steel at elevated temperatures. Journal of Constructional Steel Research, 2022, 191:

107192
49. Ren C, Dai L, Huang Y, He W. Experimental investigation of post-fire mechanical properties of Q235 cold-formed steel. Thin-walled Structures, 2020, 150: 106651
50. Qiang X, Bijlaard F S K, Kolstein H. Post-fire mechanical properties of high strength structural steels S460 and S690. Engineering Structures, 2012, 35: 1–10
51. Yu Y, Lan L, Ding F, Wang L. Mechanical properties of hot-rolled and cold-formed steels after exposure to elevated temperature: A review. Construction & Building Materials, 2019, 213: 360–376
52. Dolzhenkov I E. The nature of blue brittleness of steel. Metal Science and Heat Treatment, 1971, 13(3): 220–224
53. Zhang C, Jia B, Wang J. Influence of artificial cooling methods on post-fire mechanical properties of Q355 structural steel. Construction & Building Materials, 2020, 252: 119092
54. Zhou X, Xue X, Shi Y, Xu J. Post-fire mechanical properties of Q620 high-strength steel with different cooling methods. Journal of Constructional Steel Research, 2021, 180: 106608
55. EN 1993. Eurocode 3—Design of steel structures—Part 1-1: General rules and rules for buildings. Brussels: European Committee for Standardization, 2005
56. Wang W, Liu T, Liu J. Experimental study on post-fire mechanical properties of high strength Q460 steel. Journal of Constructional Steel Research, 2015, 114: 100–109
57. Cottrell A H, Dexter D L. Dislocations and plastic flow in crystals. American Journal of Physics, 1954, 22(4): 242–243
58. Koyama M, Shimomura Y, Chiba A, Akiyama E, Tsuzaki K. Room-temperature blue brittleness of Fe–Mn–C austenitic steels. Scripta Materialia, 2017, 141: 20–23
59. Yang X, Zhang B. Material embrittlement in high strain-rate loading. International Journal of Extreme Manufacturing, 2019, 1(2): 022003
60. Koşatepe A, Yazici C. Investigation of mechanical properties of steel reinforcements in reinforced concrete structures as a result of exposure to fire. Challenge Journal of Structural Mechanics, 2023, 9(2): 68–76
61. Gunalan S, Mahendran M. Experimental investigation of post-fire mechanical properties of cold-formed steels. Thin-walled Structures, 2014, 84: 241–254
62. Tao Z, Wang X Q, Hassan M K, Song T Y, Xie L A. Behaviour of three types of stainless steel after exposure to elevated temperatures. Journal of Constructional Steel Research, 2019, 152: 296–311
63. Zhou H, Wang W, Wang K, Xu L. Mechanical properties deterioration of high strength steels after high temperature exposure. Construction & Building Materials, 2019, 199: 664–675
64. Zhang C, Wang R, Song G. Post-fire mechanical properties of Q460 and Q690 high strength steels after fire-fighting foam cooling. Thin-walled Structures, 2020, 156: 106983
65. Yazici C, Özkal F M, Orhan S N, Cirpici B K. Reformative effects of intumescent coating on the structural characteristics of cold-formed steel. ACS Omega, 2022, 7(46): 42560–42569